Single-photon nonlinearities using arrays of cold polar molecules

R. M. Rajapakse,[1] T. Bragdon,[1] A. M. Rey,[2] T. Calarco,[3] and S. F. Yelin[1,4]
[1]*Department of Physics, University of Connecticut, Storrs, Connecticut 06269, USA*
[2]*JILA, National Institute of Standards and Technology, University of Colorado, Boulder, Colorado 80309-0440, USA*
[3]*Institute for Quantum Information Processing, University of Ulm, D-89069 Ulm, Germany*
[4]*ITAMP, Harvard-Smithsonian Center for Astrophysics, Cambridge, Massachusetts 02138, USA*
(Received 26 February 2009; revised manuscript received 2 June 2009; published 15 July 2009)

We model single-photon nonlinearities resulting from the dipole-dipole interactions of cold polar molecules. We propose utilizing "dark state polaritons" to effectively couple photon and molecular states; through this framework, coherent control of the nonlinearity can be expressed and potentially used in an optical quantum computation architecture. Due to the dipole-dipole interaction the photons pick up a measurable nonlinear phase even in the single-photon regime. A manifold of protected symmetric eigenstates is used as basis. Depending on the implementation, major sources of decoherence result from nonsymmetric interactions and phonon dispersion. We discuss the strength of the nonlinearity per photon and the feasibility of this system.

DOI: 10.1103/PhysRevA.80.013810 PACS number(s): 42.50.Dv, 03.65.Ud, 03.67.Mn

I. INTRODUCTION

Coherent control of optical nonlinearities at the single-photon level is a burgeoning topic in quantum optics research. Utilizing state-preserving techniques, it is suggested that one can implement two-qubit quantum logic gates in a feasibly robust optical quantum computational framework [1,2].

Cold polar molecules are excellent candidates as a mediating medium due to their field-dependent intermolecular interaction properties [3–7]. They have been suggested for quantum computation architectures since they embody advantages of both neutral atoms and trapped ions, viz. long coherence times and strong interactions, respectively.

Advances in preparation (cooling and trapping) of molecular ensembles in their electronic, vibrational, and rotational ground states [8] would allow for single state manipulation in a characteristically rich level structure. Notably, recent work by Büchler *et al.* [9] predicts novel, controllable superfluid, and crystalline phase transitions from dipolar gases. The latter could suppress dephasing from short-range collisions in high-density traps. The anisotropic and long-range form of the dipole-dipole interaction is responsible for the bulk of advances in controlling molecular samples [5].

In this paper, we investigate cold polar molecular gases in one- and two-dimensional arrays. We describe single-photon nonlinearities resulting from the intermolecular dipole-dipole interaction. We apply "slow" and "stored" light methodology for coherent state transfer. Next we calculate the resultant nonlinear phase in the context of collective excitations in an optically thick media.

Here we are primarily concerned with exploring feasibility of coherent control over the resultant nonlinear phase evolution of intermolecular dipole-dipole interactions. Familiar implementations for the system under discussion include stripline cavities, optical lattices, Wigner crystals, hollow fibers, or molecules on surfaces. Then, we investigate the most significant decoherence effects for implementation in a trap architecture or in a crystalline phase.

II. SINGLE-PHOTON NONLINEARITY

Photons do not interact. However, effective interaction can be achieved by utilizing state-preserving light-matter couplings to nonlinear media, wherein matter-matter interactions effectuate photon-photon interactions without destroying the state information of the incident coherent fields.

The proposed mechanism is as follows: photons are efficiently and coherently coupled into the molecular medium in the form of "slow-light polaritons." The molecule part of these light-molecule coupled excitations is "switched" from the zero-dipole rotational ground state into a high-dipole rotational superposition state. The resulting dipole-dipole interaction therefore adds a nonlinear phase to the polaritons that the photons retain on exiting the medium. We note that the nonlinear phase is thus proportional to the interaction time inside the medium and thus to the propagation time of the polaritons. Therefore control over the phase is exercised by manipulating the propagation velocity of the light in the medium.

Electromagnetically induced transparency (EIT)-based slow-light polaritons [10,11] are collective states of matter-light superposition that can be achieved by using a Λ-type system. Polaritons are the coupled exchanges of the signal field Ω_s and the superposed $|g\rangle$ and $|e\rangle$ ground states (see Fig. 1). $|g\rangle$ and $|e\rangle$ would typically be the $|J,M_J\rangle$ rotational states of the ground-state molecules, where M_J is the projection of J on the z axis. The coupling field Ω_c controls the slow group velocity of the polaritons.

The interacting states $|g\rangle$ and $|e\rangle$ in our system are neighboring rotational levels of dipolar molecules. Since dipolar interactions exchange virtual photons, interacting states must have opposite parity. This can be accomplished via an expanded Λ-type system with a strong Raman transition involving a two-photon transition as Ω_c, or alternatively the use of mixed-parity states for the excited state $|a\rangle$. For simplicity we refer to the whole molecular system as an effective two-level system, consisting of $|e\rangle$ and $|g\rangle$, as is usually done in the context of slow-light polaritons [10]. We adopt a natural shorthand, $|g_i\rangle$ and $|e_i\rangle$, respectively, for the ground and excited state of the ith molecule.

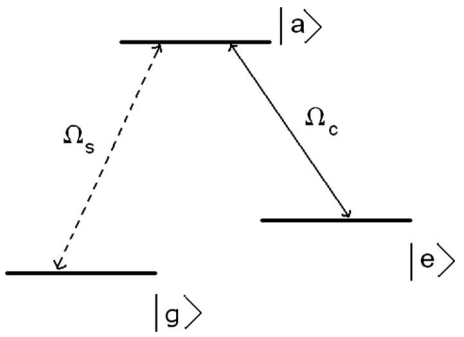

FIG. 1. Level scheme for utilizing slow-light polaritons. $|e\rangle$ and $|a\rangle$ can be coupled via a two-photon transition, or $|e\rangle$ can be a mixed-parity state.

It is convenient to introduce collective states denoted as $|j,m\rangle$. These states are eigenstates of the collective operators $\hat{J}^2$ and $\hat{J}_z$, where $\hat{J}_\alpha=\frac{1}{2}\Sigma_i\hat{\sigma}_i^\alpha$, $\alpha=x,y,z$ and $\hat{\sigma}_i^\alpha$ are Pauli operators acting on the ith molecule: $\hat{\sigma}_i^x=|g_i\rangle\langle e_i|+|e_i\rangle\langle g_i|$, $\hat{\sigma}_i^y=i(|g_i\rangle\langle e_i|-|e_i\rangle\langle g_i|)$, $\hat{\sigma}_i^z=|e_i\rangle\langle e_i|-|g_i\rangle\langle g_i|$. $|j,m\rangle$ states satisfy the eigenvalue relations $\hat{J}^2|j,m\rangle=j(j+1)|j,m\rangle$ and $\hat{J}_z|j,m\rangle=m|j,m\rangle$, with $j=N/2,\ldots,0$ and $-j\leq m\leq j$.

Among these states we are particular interested in the fully symmetric Dicke-like states which lie on the surface of the Bloch sphere with maximal radius $j=N/2$ and are totally symmetric, i.e., invariant with respect to particle permutations. We denote them as $|n\rangle=|N/2,-N/2+n\rangle$ to emphasize that they correspond to n-photon collective excitation. The corresponding $n=0,1,2$ are explicitly given by

$$|0\rangle=|g_1,\ldots,g_N\rangle,$$

$$|1\rangle=\frac{1}{\sqrt{N}}\sum_{i=1}^{N}|g_1,\ldots,e_i,\ldots,g_N\rangle,$$

$$|2\rangle=\sqrt{\frac{2}{N(N-1)}}\sum_{i<j}|g_1,\ldots,e_i,\ldots,e_j,\ldots,g_N\rangle. \quad (1)$$

In our case, cold polar molecular gases e.g., SrO [3] or CaF [12] constitute the nonlinear medium. The nonlinearity is expressed through dipole-dipole interactions. Imagine first the ideal case when such interactions between molecules generate an effective Hamiltonian of the type

$$\hat{V}_{dd}=\chi\hat{J}_z^2. \quad (2)$$

Since the states $|n\rangle$ are eigenstates of $\hat{V}_{dd}$, the collective dynamics can be fully accounted for by their phase evolution θ_n,

$$\hbar\theta_n(t)=\langle n|\hat{V}_{dd}t|n\rangle=\chi(N/2-n)^2t. \quad (3)$$

In general to characterize the medium nonlinearity we would have to include photon coupling states with $n>2$, but in the scheme of optical quantum computation it is sufficient to implement two-qubit controlled phase operation—provided appropriate single qubit gates. The latter can be realized if the accumulated nonlinear phase $\Theta(t)$ acquired by the polaritons equals π at the time when they exit the medium. $\Theta(t)$ is the difference between the phase picked up by two concurrent excitations and the sum of the phases that each individual excitation would independently pick up in the absence of the other. It is defined as

$$\Theta(t)=[\theta_2(t)-\theta_0(t)]-2[\theta_1(t)-\theta_0(t)]=\theta_2-2\theta_1+\theta_0. \quad (4)$$

In other words, $\Theta(t)$ quantifies the departure from a linear regime, that is, one in which the interaction between the two excitations is absent and therefore their individual phases simply sum up. From Eq. (2) the latter condition is satisfied if $2\chi t_\pi=\hbar\pi$. Therefore in this ideal case establishing a deterministic controlled phase operation only requires coherent control of the propagation and/or storage time of the polariton in the dipolar medium. This corresponds to manipulating the control fields that establish the conditions for the "slow-light" propagation.

However, dipolar interactions do not generate a Hamiltonian of the type described by Eq. (2) and instead the dipole-dipole interaction is given by

$$\hat{V}_{dd}^{(1D)}=\frac{1}{8\pi\epsilon_0}\sum_{i\neq j}\frac{\hat{\boldsymbol{\mu}}_i\cdot\hat{\boldsymbol{\mu}}_i-3(\hat{\boldsymbol{\mu}}_i\cdot\boldsymbol{r}_j^0)(\hat{\boldsymbol{\mu}}_j\cdot\boldsymbol{r}_i^0)}{|\boldsymbol{r}_i^0-\boldsymbol{r}_j^0|^3}, \quad (5)$$

with $\boldsymbol{\mu}_i$ the dipole moment of the molecule at site $\boldsymbol{r}_i^0$. Here we have assumed that the molecules are at fixed positions determined for example by a superimposed external optical lattice potential.

For the simplest situation when both $|g\rangle$ and $|e\rangle$ states are pure rotational states and have zero dipole moment $\boldsymbol{\mu}_{gg}=\boldsymbol{\mu}_{ee}=\mathbf{0}$, the dipole-dipole interaction is governed by the $|g\rangle\leftrightarrow|e\rangle$ transition dipole moment which can be formally written as

$$\hat{\boldsymbol{\mu}}_i=\boldsymbol{\mu}_{ge}|g_i\rangle\langle e_i|+\boldsymbol{\mu}_{eg}|e_i\rangle\langle g_i|\equiv\boldsymbol{\mu}_{ge}\hat{\sigma}_i^-+\boldsymbol{\mu}_{eg}\hat{\sigma}_i^+, \quad (6)$$

with $\boldsymbol{\mu}_{ab}\equiv\mu_0\langle a|\boldsymbol{e}_r|b\rangle$. Assuming the interacting dipoles are aligned in parallel, which is possible in one-dimensional (1D) and two-dimensional (2D) geometries, this leads to $(\hat{\boldsymbol{\mu}}_i\cdot\boldsymbol{r}_j^0)=\mathbf{0}$, and neglecting counter-rotating terms $\hat{\sigma}_i^+\hat{\sigma}_i^+$, $\hat{\sigma}_i^-\hat{\sigma}_i^-$ the interaction potential becomes

$$\hat{V}_{dd}=\frac{|\mu_{eg}|^2}{8\pi\epsilon_0}\sum_{i\neq j}\frac{\hat{\sigma}_i^+\hat{\sigma}_j^-+\hat{\sigma}_i^-\hat{\sigma}_j^+}{|\boldsymbol{r}_i^0-\boldsymbol{r}_j^0|^3}. \quad (7)$$

$\hat{V}_{dd}$ is not SU(2) symmetric and consequently the collective Dicke states are not eigenstates of it. Exceptions are $|0\rangle$ and $|1\rangle$ states which do remain eigenstates of $\hat{V}_{dd}$. This implies that the dynamical evolution of $|n\rangle$ for $n\geq2$ not only acquires a time-dependent phase, but in addition transitions to other states outside $j=N/2$ will take place. These transitions will affect the implementation of the phase gate which relies on remaining on the Dicke manifold.

Ignoring for the moment the "leakage" outside the Dicke states and focusing only the projection $\mathcal{P}$ of $\hat{V}_{dd}$ on the Dicke manifold, which is given by [13]

$$\mathcal{P}\hat{V}_{dd}=\chi_{\text{eff}}\hat{J}_z^2+\text{const}, \quad (8)$$

$$\chi_{\text{eff}} = \frac{2\kappa}{N(N-1)} \sum_{i \neq j} \frac{a^3}{|\boldsymbol{r}_i^0 - \boldsymbol{r}_j^0|^3},$$

where

$$\kappa = \frac{|\mu_{eg}|^2}{8\pi a^3 \epsilon_0}, \tag{9}$$

and a the lattice constant of the molecular array. Now one can estimate the propagation time required for implementing the phase gate as $t_\pi = \hbar\pi/(2\chi_{\text{eff}})$. The resulting expression gives $\chi_{\text{eff}} \propto 1/N$. It clearly shows that there is an optimization to undertake regarding the number of molecules in the array: on one hand, there must be enough molecules to create sufficient optical depth to couple-in the polaritons [14]. On the other hand, in order to maximize the nonlinearity in Eq. (10), less molecules are better.

In a one-dimensional molecular array, one can analytically evaluate the nonlinear phase factor Θ from Eq. (9). It is given by

$$\Theta^{(1D)} \approx \frac{4\kappa t \zeta[3]}{\hbar(N-1)}, \tag{10}$$

where $\zeta[3] = \lim_{N\to\infty} \sum_{i=1}^{i=N-1} i^{-3} \approx 1.2$.

Given aforementioned assumptions about dipole alignment, for the two-dimensional square lattice [17] only a change in lattice vectors $\boldsymbol{r}_i^0 = y_i \boldsymbol{e}_y + z_i \boldsymbol{e}_z$ is required. In this case and assuming periodic boundary conditions one obtains

$$\Theta^{(2D)} \approx 2\Theta^{(1D)}. \tag{11}$$

III. DECOHERENCE

A. Decay out of symmetric manifolds

Decay out of symmetric manifolds and phononlike effects in the Wigner crystal implementations can be significant. We will discuss symmetric manifolds at present, leaving the phononlike decoherence effects to a later section.

As mentioned in previous session, Dicke states are a good basis only if the relevant Hamiltonian is spherically symmetric [SU(2) symmetric]. This is not the case for $\hat{V}_{dd}$, and in particular the state $|2\rangle$ will decay during the time evolution inducing decoherence.

To estimate the decay probability from an initial Dicke eigenstate during the dynamical evolution we calculate the fidelity $F(t)$

$$F(t) = \frac{|\langle \psi(t)|2\rangle|^2}{|\langle \psi(0)|2\rangle|^2}, \tag{12}$$

where $|\psi(t)\rangle = -\frac{i}{\hbar}\hat{V}_{dd}|\psi(t)\rangle$, is the time evolving state under $\hat{V}_{dd}$ and $|\psi(0)\rangle = C_2(0)|2\rangle + C_1(0)|1\rangle + C_0(0)|0\rangle$. This quantity is plotted for two different 1D sample sizes in Fig. 2. In the same figure we also show the nonlinear phase Θ accumulated by the evolving state. We numerically evaluated it as

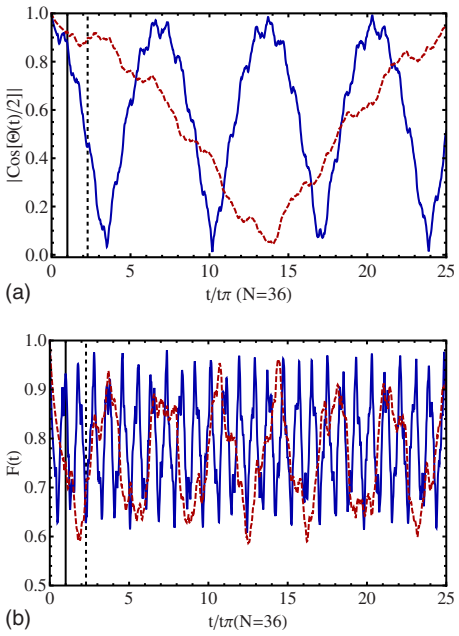

FIG. 2. (Color online) (a) Nonlinear phase as a function of time for a 1D array with $N=36$ molecules (solid line) and $N=81$ (dashed line). Here $t_\pi(N=36) = \hbar\pi/(2\chi_{\text{eff}})$ is the expected phase gate time for the $N=36$ system calculated by projecting the dipole Hamiltonian [Eq. (5)] onto the Dicke manifold. It is obvious from this graph that the projected $\Theta = \pi$ phase time ($t = t_\pi$, solid black line for $N=36$, broken for $N=81$) deviates strongly from the exact one ($t \approx 3.5 t_\pi$). The main reason for this deviation is the importance of transition processes *out of the Dicke manifold* as confirmed in panel (b) where we plot the fidelity to stay in the state $|2\rangle$.

$$\cos[\Theta(t)/2] = \frac{C_0^*(t)C_2(t) + [C_0^*(t)C_1(t)]^2}{2}, \tag{13}$$

where $C_n(t) = [\langle \psi(t)|n\rangle]/\langle \psi(0)|n\rangle$ are the projections of the evolving state into the corresponding Dicke states. The relevance of decoherence effects and the departure of the pure phase accumulation can be clearly observed in Fig. 2. The plot shows not only a distorted evolution of the nonlinear phase but also a different time dynamics since the nonlinear phase approaches π at a time very different from the expected t_π [see Eq. (10)].

One could effectively remove the mixture of j manifolds and improve the fidelity of the phase gate by the addition of an external electric field. This procedure, which we will describe in the following section, generally establishes a many-body protected manifold (MPM) [13] which helps to eliminate or mitigate decoherence effects.

B. Phononlike effects

In the presence of an external dc field, which induce repulsive dipole-dipole interactions in the ground and excited states, $(\mu_{gg}, \mu_{ee} \neq 0)$, molecules can assemble themselves in a Wigner crystal. Attractive interactions along the remaining directions can be suppressed by a strong transverse confinement [9]. In a Wigner crystal implementation, there exists another notable decoherence effect, which can be analyzed

using a phonon formalism, cf. [15]. In a realistic crystalline phase, the molecules are not fixed frozen. Phononlike effects will add to the decay described in the previous section as their energy provides a coupling between the symmetric and nonsymmetric states. Details of decoherence due to phonons will also be treated in subsequent sections.

C. Finite pulse effects

In the previous analysis we have assumed that Dicke states are the result of the coherent light-molecule interactions. However finite pulse effects can introduce inhomogeneity and can lead to nonzero initial population of states out-side the Dicke manifold. The latter will cause additional decoherence and will degrade the phase gate. The corrections can be quantitatively understood by noticing that while slow-light polaritons have linear dispersion in a linear medium, the nonlinear interaction adds a dispersion relation,

$$E(\boldsymbol{k}) = \hbar\omega_{\boldsymbol{k}} = \kappa \sum_j \frac{4}{|\boldsymbol{r}_0^0 - \boldsymbol{r}_j^0|^3} \sin^2\left(\frac{1}{2}\boldsymbol{k}\cdot\boldsymbol{r}_j^0\right). \tag{14}$$

For 1D, Eq. (14) can be rewritten as

$$\hbar\omega_{k\to 0}^{1D} \to \kappa[(-3 + 2\ln ka)(ka)^2 + O(k)^3]. \tag{15}$$

The nonlinear terms in k present in the 1D dispersion relation will degrade the phase gate. They however can be mitigated by using long pulses or a (ring) cavity, where $k=0$.

In 2D on the contrary the low energy excitations scale as

$$\hbar\omega_{k\to 0}^{2D} \to 3.27\kappa|\mathbf{k}a| \tag{16}$$

showing that in the 2D case, at least in the long-wave limit, the spectrum remains linear and thus decoherence due to finite pulse effects becomes less important.

IV. MANYBODY PROTECTED MANIFOLD

As the next step, we include a tunable dc electric field which thereby induces a dipole moment in the ground and excited states of the molecule ($\mu_{gg}, \mu_{ee} \neq 0$). This effect then augments the dipole-dipole interaction among our collective Dicke-like states in a way that enables perturbative treatment of the nonspherically symmetric part of the interaction, thus reinstating $|j,m\rangle$ as good eigenstates for the system,

$$\hat{V} = H_H + H_I = = \frac{\kappa}{2}\sum_{i\neq j} \frac{a^3}{|\boldsymbol{r}_i^0 - \boldsymbol{r}_j^0|^3}\hat{\boldsymbol{\sigma}}_i\cdot\hat{\boldsymbol{\sigma}}_j - \frac{\xi}{2}\sum_{i\neq j}\frac{a^3}{|\boldsymbol{r}_i^0 - \boldsymbol{r}_j^0|^3}\hat{\sigma}_i^z\hat{\sigma}_j^z,$$

where

$$\xi = \frac{|\mu_{eg}|^2 - \frac{1}{2}(\mu_{ee} - \mu_{gg})^2}{8\pi a^3 \epsilon_0}. \tag{17}$$

Here H_H is the spherically symmetric (Heisenberg) part of the Hamiltonian V, and H_I is the nonsymmetric (Ising) part.

If at $t=0$ an initial state is prepared within the $j=N/2$ manifold, a perturbative analysis predicts that for times t such that $\kappa t/\hbar < \xi/\kappa$, $\hat{H}_H$ confines the dynamics to the Dicke manifold and transitions outside it can be neglected. In other words the Dicke manifold becomes protected by the many-body interactions and only the projection of $\hat{H}_I$ on it, which corresponds to $\mathcal{P}\hat{H}_I = -\tilde{\chi}_{\text{eff}}\hat{J}_z^2 + \text{const}$, with $\tilde{\chi}_{\text{eff}} = \frac{\xi}{\kappa}\chi_{\text{eff}}$ becomes effective. As a consequence H_I acts as the desired ideal "phase gate" Hamiltonian.

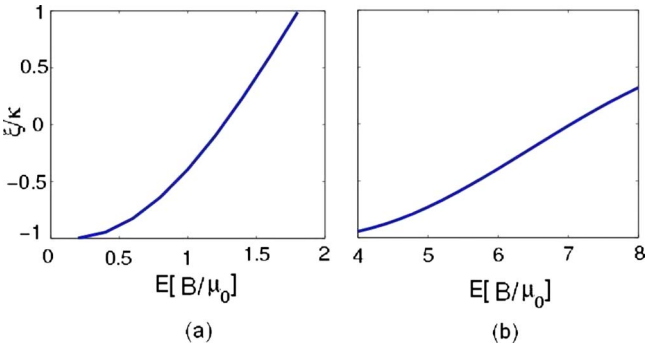

FIG. 3. (Color online) ξ/κ for varying $E[B/\mu_0]$ in SrO. (a) $|g_i\rangle = |J_{\text{SrO}}, M_{J,\text{SrO}}\rangle = |0,0\rangle_i$ and $|e_i\rangle = |1,0\rangle_i$. (b) $|g_i\rangle = |1,0\rangle_i$ and $|e_i\rangle = |2,0\rangle_i$. B is the rotational constant of the molecule, and μ_0 is the maximum ground-state dipole moment, in our case assumed to be $\mu_0 = |\boldsymbol{\mu}_{eg}|$.

The relative strength of the H_H and H_I parts of $\hat{V}$ can be manipulated to find values of ξ/κ such that MPM protection is maximized. For example, SrO has a $^1\Sigma$ ground state with a magnetic moment of 8.89D. Upon selecting ground and excited rotational states with opposing parity, the appropriate values of ξ and κ are then obtained by diagonalizing the Stark Hamiltonian for variable electric fields [15]. In Fig. 3, we show the ratio of ξ/κ for varying dc field strength between two rotational levels of SrO. For induced dipole transitions, the biasing electric dc field E depends on both the rotational constant B and the ground-state dipole moment μ_0.

The application of an electric field changes the original bare states to dressed states $|g\rangle$ and $|e\rangle$ which are linear superpositions of the bare states. It has to be noted that the addition of a dc field, leading to MPM protection, causes the nonlinearity to be reduced by a factor of $\sim|\xi/\kappa|$.

Decay out of manybody protected manifold into other manifolds

In this section we study what occurs if at time $t=0$ we prepare the system in the $j=N/2$ subspace and let the system evolve in time in the presence of MPM. This can be written as

$$|\Psi_n(t)\rangle = e^{-1/2\gamma_n(t)t}e^{-i\theta_n(t)}|N/2, -N/2+n\rangle. \tag{18}$$

Here we estimate the decay magnitude γ_n. Our objectives are to keep θ_n large while minimizing γ_n. As the states with 0 and 1 excitations are eigenstates of the symmetric manifold there is no decay out of the manifolds and therefore $\gamma_0 = 0$ and $\gamma_1 = 0$.

Using first-order perturbation theory we can write

$$e^{-\gamma_2(t)t} \simeq 1 - \frac{1}{\hbar}\sum_{k,k'>0}\left|\int_0^t d\tau \mathcal{M}_{k,k'}e^{i\tau(\omega_k+\omega_{k'})}\right|^2. \tag{19}$$

The quantities $\mathcal{M}_{k,k'} = \langle N/2, -N/2+2|H_I|\psi_{k,k'>0}\rangle$ are the transition matrix elements to states with $j=N/2-2$ which are

the only ones which couple to $|2\rangle$ according to the Wigner-Eckart theorem. To a good approximation they are given by $|\psi_{\boldsymbol{k},\boldsymbol{k}'}\rangle = \frac{1}{\sqrt{N(N-1)}}\Sigma_{i\neq j} e^{i(\boldsymbol{k}\cdot\boldsymbol{r}_j^0 + \boldsymbol{k}'\cdot\boldsymbol{r}_i^0)}\sigma_j^-\sigma_i^-|0\rangle$ and their corresponding excitation energies by $\hbar(\omega_{\boldsymbol{k}}+\omega_{\boldsymbol{k}'})$, with $\omega_{\boldsymbol{k}}$ given by Eq. (14). $\hbar\boldsymbol{k}$, $\hbar\boldsymbol{k}'$ are discrete quasimomenta, which for a 2D square lattice with lattice spacing a can be written as $\boldsymbol{k} = \frac{2\pi}{a\sqrt{N}}(i,j)$, $i,j=0,\ldots,N-1$. Note that the sum over $\boldsymbol{k},\boldsymbol{k}'$ in $\mathcal{M}_{\boldsymbol{k},\boldsymbol{k}'}$ excludes the state $\boldsymbol{k}=\boldsymbol{k}'=\boldsymbol{0}$ since $\psi_{\boldsymbol{0},\boldsymbol{0}}$ is just $|2\rangle$.

After some algebra, one can show that $\mathcal{M}_{\boldsymbol{k},\boldsymbol{k}'} = \frac{4\xi}{N}F_{\boldsymbol{k}}\delta_{\boldsymbol{k},-\boldsymbol{k}'}$ where $F_{\boldsymbol{k}}$ is the Fourier series of $|\boldsymbol{r}_i^0 - \boldsymbol{r}_j^0|^{-3}$, i.e., $F_{\boldsymbol{k}} = a^3\Sigma_j |\boldsymbol{r}_0^0 - \boldsymbol{r}_j^0|^{-3}\cos(\boldsymbol{k}\cdot\boldsymbol{r}_j^0)$. Replacing the latter equation in Eq. (19) yields the following expression for the decay rate:

$$e^{-\gamma_2(t)t} \simeq 1 - \frac{16\xi^2}{N^2}\sum_{\boldsymbol{k}>0}|F_{\boldsymbol{k}}|^2\frac{\sin^2(\omega_{\boldsymbol{k}}t)}{\hbar^2\omega_{\boldsymbol{k}}^2}. \tag{20}$$

To get a general idea on the decay rate behavior we first use Fermi's golden rule to estimate the decay rate in the thermodynamic limit, $N\to\infty$ and then we compare these predictions with numerical studies for finite-size systems. According to Fermi's golden rule, at long times the decay probability evolves linear with time as $\gamma_2(t)=\Gamma_2$,

$$\Gamma_2 \simeq \frac{4\pi\xi^2}{\hbar N}\int \frac{(ad\boldsymbol{k})^D|F_{\boldsymbol{k}}|^2}{(2\pi)^D|\nabla_{\boldsymbol{k}}\omega_{\boldsymbol{k}}|}\delta(a\boldsymbol{k}). \tag{21}$$

The latter relation yields that $\Gamma_2 t_\pi$ diverges in 1D as

$$\Gamma_2 t_\pi \propto \frac{\xi}{\kappa}\int d(ka)\frac{\delta(ka)}{|ka\,\log\,ka|} \to \infty,$$

implying the break down of Fermi's golden rule approximation and emphasizing the issue that in 1D nonsymmetric decoherence effects are crucial in the large N limit.

In 2D, the situation is better due to the linear dependence of the long-wave excitations with k and the extra factor of k in the density of states. This yields that

$$\Gamma_2 t_\pi \propto \frac{\xi}{\kappa}\int d(ka)ka\,\delta(ka) \to 0$$

and

$$F^{2D}(t_\pi) \to 1, \tag{22}$$

Consequently as long as $\xi<\kappa$ (which is required for the validity of our perturbative treatment) and neglecting other decoherence effects during the time evolution (which grows linearly with N) Fermi's golden rule predicts a robust phase gate in 2D.

To validate these predictions we solve the exact many-body dynamics numerically by evolving a system initially prepared in the Dicke state with $n=2$ under the effective Hamiltonian $\hat{V}$, and compute the fidelity, $\mathcal{F}$ of remaining in a Dicke state,

$$\mathcal{F}(t) = |\langle N/2,-N/2+2|\Psi(t)\rangle|^2 = e^{-\gamma_2(t)t}. \tag{23}$$

In Fig. 4 we show the 1D dynamics using the parameters $\xi/\kappa=0.05$ and $N=36$ and 81 and plot both Θ and $F(t)$. Note in the presence of the MPM, the time when the phase gate is implemented is close to the expected time t_π. Figure 4 confirms the prediction that in 1D the fidelity decreases with increasing N. We find that for moderate N the 1D decay probability increases as $\approx 0.01\frac{\xi^2}{\kappa^2}N^{1.62}$, which is obtained via a fit. This relation implies that in order to implement a robust gate

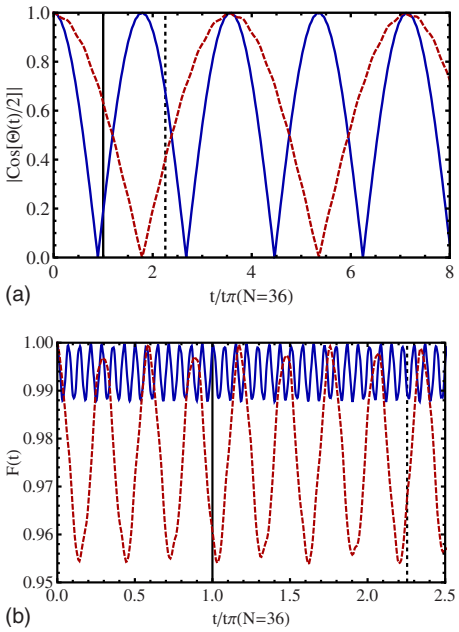

FIG. 4. (Color online) (a) Nonlinear phase as a function of time for a 1D array with $N=36$ molecules (solid line) and $N=81$ (dashed line) in the presence of an external dc field, $\xi/\kappa=0.05$. The latter is used to implement the MPM. Here $t_\pi(N=36)=\hbar\pi/(2\tilde{\chi}_{\text{eff}})$ is the expected phase gate time from our perturbative analysis for the $N=36$ system (indicated by a solid grid line). The corresponding time for the $N=81$ system is indicated by the dashed vertical line. For the two cases the actual time at which the phase gate is accomplished, $|\cos(\Theta/2)|=0$ is close to the calculated t_π indicating the validity of the perturbative analysis specially for $N=36$. The deviations can be accounted for by higher order corrections in perturbation theory. The fidelity of remaining in the $|2\rangle$ state is shown in panel b. The latter decreases as either the ratio ξ/κ or N increases, consistently with Fermi's golden rule predictions.

$$\frac{\xi^2}{\kappa^2} \ll \frac{100}{N^{1.62}}. \tag{24}$$

However, by choosing ξ/κ small we pay the price of having slower dynamics and therefore we make the system more vulnerable to other type of losses.

Figure 5 emphasizes the gain in fidelity obtained by going from 1D to 2D. With the same number of molecules and even a much larger $\xi/\kappa=1$ the fidelity is much better than in 1D. By numerically evaluating the maximum decay probability we find it behaves as $\propto\frac{\xi^2}{\kappa^2}N^{-0.86}$. The decrease in F with increasing N is in agreement with Fermi's golden rule approximation.

V. WIGNER CRYSTAL AND PHONONS

In dense low-temperature systems with sufficiently strong fixed dc electric fields [9], one can realize a self-ensemble

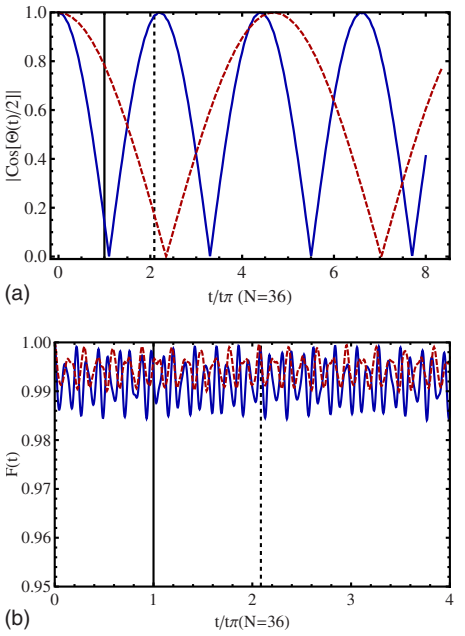

FIG. 5. (Color online) (a) Nonlinear phase as a function of time for a 2D array with $N=36$ molecules (solid line) and $N=81$ (dashed line). The solid and dashed vertical lines indicated the expected phase gate time according to our perturbative analysis. The ratio of $\xi/\kappa=1$ is outside the perturbative regime however the dynamics exhibits almost the behavior expected from an ideal $\hat{J}_z^2$ evolution. The fidelity to remain in the $|2\rangle$ state is shown in panel b. Note that in 2D the fidelity improves as N is increased.

molecular crystal or Wigner crystal. In this crystalline phase $|\mu_{gg}|>0$ and the molecules are localized at their classical equilibrium positions, $\boldsymbol{r}_i^0$. The latter form a linear chain in 1D or a triangular lattice in 2D, with lattice spacing a. The formation of a Wigner crystal is fundamentally determined by the dimensionless parameter

$$\beta = \frac{(\text{potential energy})}{(\text{kinetic energy})} \equiv \frac{U_{dd}}{\hbar^2/(ma^2)}, \tag{25}$$

for molecules of mass m for a given density $\rho=1/(a)^D$. For $\beta \gg 1$ the dipolar repulsion wins over kinetic energy stabilizing the crystalline phase. In contrast to the case where the localization of the molecules is enforced by an external potential such as an optical lattice, in the self-assembled crystalline phase, molecules are not frozen and they can exhibit collective oscillations (phonons) about their equilibrium positions. These oscillations can be described by rewriting the position operators as $\boldsymbol{r_i}=\boldsymbol{r_i^0}+\boldsymbol{x_i}$ and expanding V in powers of $\boldsymbol{x_i}$. This procedure yields three terms: the fixed position dipolar Hamiltonian [Eq. (18)] described in the prior sections, the phonon Hamiltonian which is gapless (see Appendix A) and a phonon-polariton interaction Hamiltonian $V_{phon-po}$ given by

$$V_{phon-po} = -2\kappa \sum_{i\neq j} G_{ij}\vec{\sigma}_i \cdot \vec{\sigma}_j - 2\xi \sum_{i\neq j} G_{ij}\sigma_i^z\sigma_j^z + 8B_0 \sum_{i\neq j} G_{ij}(\sigma_i^z + \sigma_j^z), \tag{26}$$

where

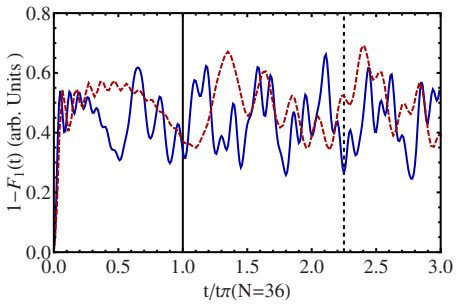

FIG. 6. (Color online) $1-F_1(t)$, where $1-F_1(t)/(\xi+4B_0)^2/\sqrt{\beta}$ is the probability of decay of a single excitation for a 1D system with $N=36$ (solid), $N=81$ (dashed) and ξ, B_0 and β are system dependant parameters. The solid and dashed vertical lines are at the time where the perturbative treatment predicts the implementation of the phase gate for the $N=36$ and 81 systems, respectively.

$$G_{ij} = -3a^3 \frac{(\mathbf{x_i}-\mathbf{x_j})\cdot(\mathbf{r_i^0}-\mathbf{r_j^0})}{4|\mathbf{r_i^0}-\mathbf{r_j^0}|^5}.$$

and $B_0=(\mu_{ee}^2-\mu_{gg}^2)/(8\pi a^3\epsilon_0)$. $V_{phon-po}$ is not spherically symmetric, Dicke states are not eigenstates of it and consequently $V_{phon-po}$ will induce transition outside the Dicke manifold even for the one-photon excitation state, $|1\rangle$. These transitions can degrade the phase gate significantly since they are not suppressed by the MPM due to the gapless nature of the phonon spectrum. If at time $t=0$ we prepare our state in the $J=N/2$ manifold, the projection of the evolving state on the n-Dicke state can be written as

$$|\Psi_n(t)\rangle = e^{-\gamma_{n,ph}(t)/2t}e^{-i\theta_n(t)}|N/2,-N/2+n\rangle, \tag{27}$$

and the decoherence rates γ_{1ph} and γ_{2ph} approximately calculated using perturbation theory [15]. This procedure yields an expression for γ_{1ph} given by

$$\gamma_{1ph} \simeq \frac{\pi(\xi+4B_0)^2}{\hbar\sqrt{\beta}} \sum_{\lambda} \int \frac{d^D(a\boldsymbol{k})}{(2\pi)^D} g_\lambda(\boldsymbol{k})\{[N(\omega_\lambda(\boldsymbol{k})) + 1]\delta(\omega_\lambda(\boldsymbol{k})-\omega_{\boldsymbol{k}}) + N(\omega_\lambda(\boldsymbol{k}))\delta(\omega_\lambda(\boldsymbol{k})+\omega_{\boldsymbol{k}})\}. \tag{28}$$

Here $N(\omega_\lambda(\mathbf{k}))=1/(e^{\hbar\omega_\lambda(\mathbf{k})/(k_BT)}-1)$ is the thermal occupation number for phonons with the phonon spectrum $\omega_\lambda(\mathbf{k})$ (see Figs. 8 and 9). See Eq. (37) for the definition of $g_\lambda(\boldsymbol{k})$. For two photon excitations it can be shown in a similar way that

$$\gamma_{2ph} \approx 2\gamma_{1ph}. \tag{29}$$

Detailed derivations are included in the Appendix B.

In Ref. [15] analytical expressions for the decay rates in the thermodynamic limit were derived using Fermi's golden rule. In this limit the decoherence induced by phonons was shown only to be relevant in 1D and proportional to the temperature. For our finite number of molecules Fermi's golden rule results are only crude approximations and for a quantitative treatment we instead perform numerical calculations which are summarized in Figs. 6 and 7. There we plot the time evolution of the decay probability for two systems with different N. We find a general tendency of the maximum decay probability to grow with increasing N specially for 1D.

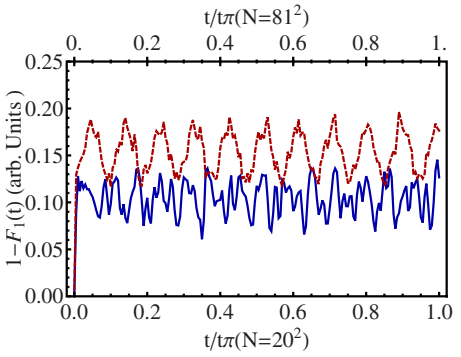

FIG. 7. (Color online) $1-F_1(t)$, where $1-F_1(t)/(\xi+4B_0)^2/\sqrt{\beta}$ is the probability of decay of a single excitation for a 2D system with $N=20^2$ (solid), $N=81^2$ (dashed) and ξ, B_0, and β are system dependant parameters. In this case we had to go to larger system sizes to show the decrease in fidelity with increasing N. The top (bottom) axis scales are for $N=81^2(20^2)$.

Also for fixed N, β, and κ we observe a linear dependence on the temperature in agreement with Fermi's golden rule predictions.

VI. CONCLUSION

In this paper, we explore the feasibility of utilizing cold polar molecules in 1D and 2D optical lattices for coherently controlled nonlinear optics. We report a controlled π phase gate time that increases proportionally to the number of interacting molecules, but also note better fidelity in 2D systems for reasonable system parameters and external field strengths. We address the role of nonsymmetric interactions, one of the major decoherence effects, and demonstrate the enhancement of phase gate fidelity when an MPM is created by applying external electric fields. For self-assembled crystalline samples, we also have explored phonon-induced decoherence. Since we find that at low temperature the most relevant decoherence effects in the Wigner crystal arrays are caused by long-wave phonon excitations, spin-echo techniques could help to reduce them.

ACKNOWLEDGMENTS

The authors wish to acknowledge NSF for funding, and Peter Rabl for fruitful discussions. Tommaso Calarco wishes to acknowledge the EC Integrated Project SCALA.

APPENDIX A: SELF-ASSEMBLED MOLECULAR CRYSTALS

In a self-assembled ensemble molecular crystal, molecules are not longer completely frozen at the classical equilibrium positions, $\boldsymbol{r}_i^0$, which form a linear chain in 1D or a triangular lattice in 2D, with lattice spacing a. Instead they exhibit collective oscillations (phonons) in the crystal. If we expand the total Hamiltonian, Eq. (7) around the equilibrium positions: $\mathbf{r_i}=\mathbf{r_i^0}+\mathbf{x_i}$ and keep terms up to quadratic order $\mathbf{x_i}$ one obtains the following expression:

$$H = H_{phon} + V + V_{phon-po}, \tag{A1}$$

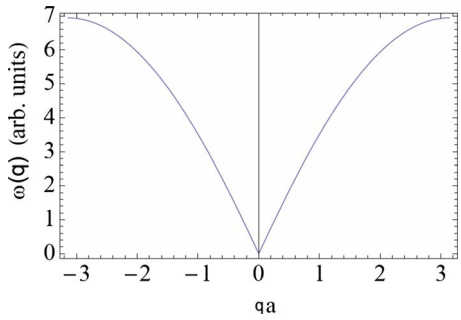

FIG. 8. (Color online) Phonon excitation spectrum in 1D. a is the separation between the molecules. The units of $\omega(q)$ are $U_{dd}/\sqrt{\beta}$.

$$H_{phon} = \sum_i \frac{\mathbf{p}_i^2}{2m} + \frac{3\mu_{gg}^2}{16\pi\epsilon_0 a^3}\sum_{i\neq j}\frac{5[(\mathbf{x_i}-\mathbf{x_j})\cdot\mathbf{n_{ij}^0}]^2-[(\mathbf{x_i}-\mathbf{x_j})]^2}{|\mathbf{r_i^0}-\mathbf{r_j^0}|^5}, \tag{A2}$$

$$= \sum_{\boldsymbol{q},\lambda}\hbar\omega_\lambda(\boldsymbol{q})\hat{a}^\dagger_{\boldsymbol{q},\lambda}\hat{a}_{\boldsymbol{q},\lambda}, \tag{A3}$$

where $\hat{a}_{\boldsymbol{q},\lambda}$ is the annihilation operator for phonons with quasimomentum $\boldsymbol{q}$ and frequency $\omega_\lambda(\boldsymbol{q})$ and $\mathbf{n_{ij}^0}$ is a unit vector along $\mathbf{r_i^0}-\mathbf{r_j^0}$. In 2D the index λ labels the two different phonon branches. In general

$$\omega_\lambda(\boldsymbol{q}) = \frac{U_{dd}}{\sqrt{\beta}} f_\lambda(\boldsymbol{q}). \tag{A4}$$

The phonon modes in the dipolar crystal are acoustic phonons, $f_\lambda(\boldsymbol{q})\sim(c_\lambda\boldsymbol{q})$. The phonon spectrum for 1D and 2D crystals is plotted in Figs. 8 and 9.

APPENDIX B: DECAY OF DIPOLAR EXCITATIONS

1. Decay of a single excitation

We start by deriving the decoherence rate γ_{1ph} for single excitations. To first order in perturbation theory we can write

$$e^{-\gamma_{1ph}(t)} \simeq 1 - \frac{2}{\hbar^2}\int_0^t dt'\int_0^{t'} d\tau \sum_{\boldsymbol{q},\lambda,\boldsymbol{k}>0}|\mathcal{L}_{\boldsymbol{k},\boldsymbol{q},\lambda}|^2 \times\{[N(\omega_\lambda(\boldsymbol{q}))+1]\cos(\Omega^+_{\boldsymbol{q},\boldsymbol{k}}\tau) + N(\omega_\lambda(\boldsymbol{q}))\cos(\Omega^-_{\boldsymbol{q},\boldsymbol{k}}\tau)\}, \tag{B1}$$

where $N(\omega_\lambda(\boldsymbol{q}))=1/(e^{\hbar\omega_\lambda(\boldsymbol{q})/(k_BT)}-1)$ is the thermal occupation number for phonons with the phonon spectrum $\omega_\lambda(\boldsymbol{q})$ (see Figs. 8 and 9) and $\Omega^\pm_{\boldsymbol{q},\boldsymbol{k}}=\omega_\lambda(\boldsymbol{q})\pm\omega_{\boldsymbol{k}}$. $\omega_{\boldsymbol{k}}$ is the dispersion relation given in Eq. (14). Here we have used the property that

$$\mathbf{x}_i = \frac{1}{\sqrt{N}}\sum_{\boldsymbol{q}}\sum_{\lambda=1}^{D}\sqrt{\frac{a^2}{2\sqrt{\beta}f_\lambda(\boldsymbol{q})}}\boldsymbol{e}_\lambda(\hat{a}_{\lambda,\boldsymbol{q}}e^{i[\boldsymbol{q}\cdot\boldsymbol{r}_i^0-\omega_\lambda(\boldsymbol{q})]t} + \hat{a}^\dagger_{\lambda,\boldsymbol{q}}e^{-i[\boldsymbol{q}\cdot\boldsymbol{r}_i^0-\omega_\lambda(\boldsymbol{q})]t}), \tag{B2}$$

where in the 2D case the vectors $\boldsymbol{e}_\lambda$ are the two orthonormal polarization vectors of the two phonon branches. $\mathcal{L}_{\boldsymbol{k},\boldsymbol{q},\lambda}$

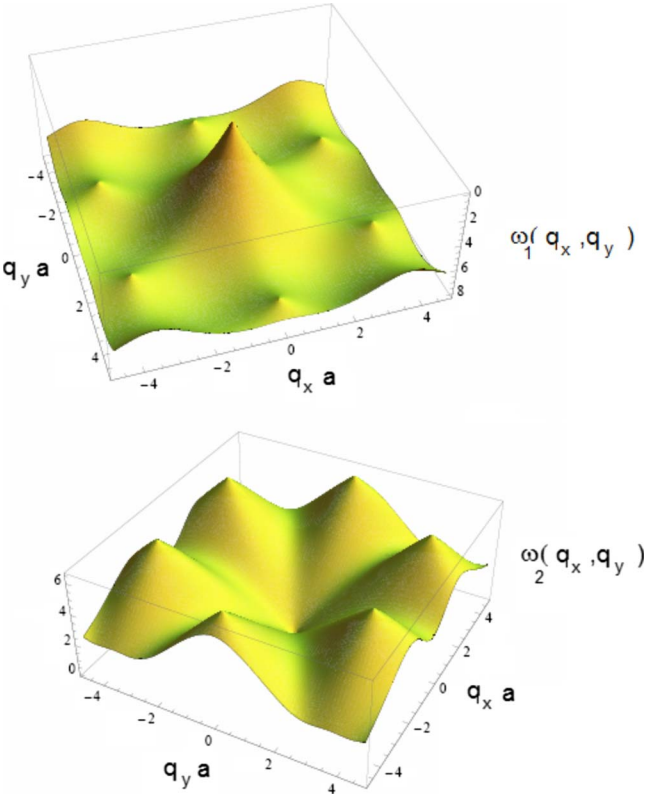

FIG. 9. (Color online) Phonon excitation spectrum in 2D for the two different branches of the phonon spectrum. q_x and q_y label the 2D quasimomenta. The units of $\omega_{1,2}(q_x,q_y)$ are $U_{dd}/\sqrt{\beta}$.

$=|\langle\psi_0|V_{phon-po}|\psi_k\rangle|$, and can be explicitly written as

$$\mathcal{L}_{k,q,\lambda} = -3\sqrt{\frac{1}{2N\sqrt{\beta}f_\lambda(q)}}\sum_{i,j}\frac{a^4[e_\lambda\cdot(r_i^0-r_j^0)]}{4|\mathbf{r_i^0}-\mathbf{r_j^0}|^5}\cdot[e^{iq\cdot r_i^0}\langle\psi_0| - \xi\sigma_i^z\sigma_j^z + 4B_0(\sigma_i^z+\sigma_j^z)|\psi_k\rangle] \tag{B3}$$

With the substitution of

$$g_\lambda(q) \equiv \frac{9}{f_\lambda(q)}\left(\sum_{i\neq 0}\left[\sin(q\cdot r_i^0)\frac{(a^4 e_\lambda\cdot r_i^0)}{|\mathbf{r_i^0}|^5}\right]\right)^2. \tag{B4}$$

Equation (36) can be simplified to

$$\mathcal{L}_{k,q,\lambda} = i\sqrt{\frac{1}{2N\sqrt{\beta}}}(\xi+4B_0)\delta_{q,-k}\sqrt{g_\lambda(q)}. \tag{B5}$$

In the regime where Fermi's golden rule is expected to be valid the decay rate is constant; $\gamma(t)=\gamma$ and following a similar procedure described in Ref. [16] one can show it is given by

$$\gamma_{1ph} \simeq \frac{\pi(\xi+4B_0)^2}{\hbar\sqrt{\beta}}\sum_\lambda\int\frac{d^D(ak)}{(2\pi)^D}g_\lambda(k)\{[N(\omega_\lambda(k)) + 1]\delta(\omega_\lambda(k)-\omega_k) + N(\omega_\lambda(k))\delta(\omega_\lambda(k)+\omega_k)\}. \tag{B6}$$

The resonance condition is defined as $[\omega_\lambda(q_0^\pm)\pm\omega_{q_0^\pm}]=0$ and assuming that $q_0^\pm=0$ is the only possible solution, the decay rate is determined by the $k\to 0$ limit of the integrant in Eq. (39) which is given in 1D by

$$\gamma_{1ph}^{1D} \sim \frac{(\xi+4B_0)^2}{4}\sqrt{3\zeta(3)}\sqrt{\beta}k_BT. \tag{B7}$$

Due to the finite value of γ_{1ph}^{1D}, and the linear dependence on N of t_π the probability of remaining on the symmetric manifold decreases exponentially with N and decoherence due to phonons is certainly a limiting factor.

On the other hand in 2D, the decay rate vanishes as

$$\gamma_{1ph}^{2D} \propto \lim_{q\to 0}(\xi+4B_0)^2k_BTq \to 0. \tag{B8}$$

This conclusion however is only a rough estimation and our numerical simulations shows that phonons can induce important decoherence effects in 2D even in finite crystals.

2. Decay of two dipolar excitations

In the main body of our paper we have stated that $\gamma_{2ph}\approx 2\gamma_{1ph}$. A detailed derivation is given below.

To first order in perturbation theory we can write

$$e^{-\gamma_{2ph}(t)/\hbar} \simeq 1-\frac{2}{\hbar^2}\int_0^t dt'\int_0^{t'}d\tau\sum_{q,\lambda,k,k'>0}|\mathcal{S}_{k,k',q,\lambda}|^2\{[N(\omega_\lambda(q)) + 1]\cos(\Omega^+_{q,k,k'}\tau) + N(\omega_\lambda(q))\cos(\Omega^-_{q,k,k'}\tau)\}, \tag{B9}$$

where $\Omega^\pm_{q,k,k'}=\omega_\lambda(q)\pm(\omega_k+\omega_{k'})$ and $\mathcal{S}_{k,k',q,\lambda}$ is rewritten in the same form as

$$\mathcal{S}_{k,k',q,\lambda} = -3\sqrt{\frac{1}{2N\sqrt{\beta}f_\lambda(q)}}\sum_{ij}\left\{e^{iq\cdot r_i^0}\langle\psi_0| - \xi\sigma_i^z\sigma_j^z + 4B_0(\sigma_i^z + \sigma_j^z)|\psi_{k,k'}\rangle\frac{a^4[e_\lambda\cdot(r_i^0-r_j^0)]}{4|\mathbf{r_i^0}-\mathbf{r_j^0}|^5}\right\}$$
$$= 3i\sqrt{\frac{1}{2N\sqrt{\beta}f_\lambda(q)}}\left[(\xi+4B_0)(\delta_{q,-k}\delta_{k',0}+\delta_{q,-k'}\delta_{k,0}) - \frac{4\xi}{N}\delta_{-q,k+k'}\right]\sum_{i\neq 0}\left[\sin(q\cdot r_i^0)\frac{(a^4 e_\lambda\cdot r_i^0)}{|\mathbf{r_i^0}|^5}\right]. \tag{B10}$$

In the above expression the term proportional to ξ/N is much smaller than the one proportional to $\xi+4B_0$ and can be neglected. Under this assumption, $\gamma_{2ph}(t)\to\gamma_{2ph}$,

$$\gamma_{2ph}\approx 2\gamma_{1ph}. \tag{B11}$$

[1] M. D. Lukin, M. Fleischhauer, R. Côté, L. M. Duan, D. Jaksch, J. I. Cirac, and P. Zoller, Phys. Rev. Lett. **87**, 037901 (2001).
[2] I. Friedler, D. Petrosyan, M. Fleischhauer, and G. Kurizki, Phys. Rev. A **72**, 043803 (2005).
[3] D. DeMille, Phys. Rev. Lett. **88**, 067901 (2002).
[4] C. Lee and E. A. Ostrovskaya, Phys. Rev. A **72**, 062321 (2005).
[5] D. Jaksch, H. J. Briegel, J. I. Cirac, C. W. Gardiner, and P. Zoller, Phys. Rev. Lett. **82**, 1975 (1999).
[6] A. Andre, J. M. Doyle, D. DeMille, M. D. Lukin, S. E. Maxwell, and P. Rabl, Nat. Phys. **2**, 636 (2006).
[7] S. F. Yelin, K. Kirby, and R. Cote, Phys. Rev. A **74**, 050301(R) (2006).
[8] K.-K. Ni, S. Ospelkaus, M. H. G. de Miranda, A. Pe'er, B. Neyenhuis, J. J. Zirbel, S. Kotochigova, P. S. Julienne, D. S. Jin, and J. Ye, Science **322**, 231 (2008).
[9] H. P. Büchler, E. Demler, M. Lukin, A. Micheli, N. Prokof 'ev, G. Pupillo, and P. Zoller, Phys. Rev. Lett. **98**, 060404 (2007).
[10] M. Fleischhauer and M. D. Lukin, Phys. Rev. Lett. **84**, 5094 (2000).
[11] M. Lukin, Rev. Mod. Phys. **75**, 457 (2003).
[12] A. Micheli, G. Pupillo, H. P. Büchler, and P. Zoller, Phys. Rev. A **76**, 043604 (2007).
[13] A. M. Rey, L. Jiang, M. Fleischhauer, E. Demler, and M. D. Lukin, Phys. Rev. A **77**, 052305 (2008).
[14] M. Bajcsy, S. Hofferberth, V. Balic, T. Peyronel, M. Hafezi, A. S. Zibrov, V. Vuletic, and M. Lukin, e-print arXiv:0901.0336.
[15] P. Rabl and P. Zoller, Phys. Rev. A **76**, 042308 (2007).
[16] P. Rabl (private communication).
[17] For simplicity we assumed a square lattice. This assumption does not change the overall picture of the dynamics of one looks at other types of 2D lattices, such as triangular ones.